RSC Advances

PAPER

View Article Online
View Journal | View Issue

Cite this: *RSC Adv.*, 2014, **4**, 13108

Silica-diblock fluoropolymer hybrids synthesized by surface-initiated atom transfer radical polymerization†

Hongpu Huang and Ling He*

Silica/diblock fluoropolymer hybrids SiO_2-*g*-PMMA-*b*-P12FMA for coatings were synthesized by the silica surface-initiating atom transfer radical polymerization (SI-ATRP) of methylmethacrylate (MMA) and dodecafluoroheptyl methacrylate (12FMA). Silica surface initiator (SiO_2-initiator) was obtained by 10–25 nm fumed silica particles grafted hydrosilylated undec-10-enyl, 2-bromo-2-methyl propionate with a density of 0.573 mmol g^{-1}. The SI-ATRP approach in this paper displays the diagnostic criteria of controlled radical polymerization by the analysis of ^{1}H NMR, ^{19}F NMR and SEC-MALLS analysis, after comparing with the conventional initiator of ethyl 2-bromoisobutyrate (EBiB) for the E-PMMA-*b*-P12FMA diblock copolymer. Three mass ratios of SiO_2-initiator/MMA/12FMA as 1/72.50/18.15, 1/72.50/45.38 and 1/181.26/18.15 were used to obtain the SiO_2-*g*-PMMA-*b*-12FMA hybrids. The hybrids show 25–30 nm core–shell particles in $CHCl_3$ solution composed of a P12FMA core and PMMA shell, but densely twined together as agglomerated particles. The PMMA-*b*-P12FMA shell grafted onto silica particles obviously increases the surface roughness of the film (50–500 nm), more than the E-PMMA-*b*-12FMA film (30 nm), and thereby contributes to the hydrophobic (112–118°) and oleophobic (45–78°) properties of the films. Increasing the P12FMA concentration (1/72.50/45.38) could result in stronger migration of the P12FMA segments onto the film surface, and therefore led to a lower surface free energy (10.97 mN m^{-1}), increased advancing and receding for water contact angles (112° and 108°) and the highest cetane contact angles (74° and 70°), the lower water absorption and viscoelasticity, but a high thermostability at 420–450 °C.

Received 6th December 2013
Accepted 20th January 2014

DOI: 10.1039/c3ra47393g

www.rsc.org/advances

1. Introduction

Inorganic/polymeric hybrids have attracted great interest in improving the properties of nanostructured polymeric materials.[1–4] Silica is one of the most investigated inorganic particles for introducing into polymer matrices due to its easy preparation, controlled particle size and well-understood surface chemistry.[5–7] It is reported that the extreme nonwetting behavior of film surfaces could be obtained when silica particles are embedded into the surface for multiple scales of roughness and re-entrant curvature.[8,9] Therefore, silica/polymer hybrids have been extensively studied as coating materials. However, the key point in controlling the properties of final materials is how the silica particles are dispersed in the polymer matrix. One effective way is to graft polymer chains chemically onto the silica particles to avoid agglomeration.[10] This does not only improve the stability of the silica particles in suspension, but also increases the compatibility of the silica particles with the polymer matrix.

Generally, there are two approaches to chemically attach polymer chains to a silica surface:[8,11] (1) the "grafting to" method, where the end-functionalized polymers react with an appropriate surface and (2) the "grafting from" method, where polymer chains are grown from the surface of the initiators.[12] The modification of silica particles *via* the substitution of surface silanol groups with mono- or multifunctional silanes has been proven to be a reliable approach to achieve satisfactory surface coverage of the desired functional groups.[13,14] Using the grafting from approach by controlled/"living" silica surface-initiated atom transfer radical polymerization (SI-ATRP), many silica hybrid particles are synthesized, such as the growth of polystyrene (PS) from high-surface-area silica gels,[15–17] the multilayer organo–silica/polystyrene/polyaniline composite particles,[14] the core–shell silica–polypeptide composite particles,[18] the core–shell structured silica encapsulated perylenediimide (PDI) nanoellipsoids,[19] and the silica nanoparticles bearing vinyl groups and covered by fluorinated chains.[20] Therefore, the SI-ATRP technique has many advantages over conventional radical polymerizations in controlling the polymer architecture and molecular weight for obtaining hybrids.[21–24]

Department of Chemistry, School of Science, Xi'an Jiaotong University, Xianning West Road, 28, Xi'an, 710049, China. E-mail: heling@mail.xjtu.edu.cn; Fax: +86-29-82668559; Tel: +86-29-82668554

† Electronic supplementary information (ESI) available. See DOI: 10.1039/c3ra47393g

Introducing fluorine-containing substituents into a silica/polymer could result in dramatic changes in the material properties of low surface energy (typically 5 mN m^{-1}) and good chemical/thermal stability.[25–27] Their "oleophobicity" acts as a driving force for obtaining low surface free energy films and is useful from a practical point of view. It is reported that such a modification also leads to significant changes in the high thermal stability (up to 400 °C) compared to physically absorbed complexes,[28] which ensures the successful development and application of fluoroalkyl-functionalized silica hybrids in producing durable nonwetting surfaces.[29–32] On the other hand, the self-assembly of fluorinated block copolymers could produce significant thin films for coatings.[29,30] In comparison to bulk systems, self-assembled thin films (~100 nm thickness) are strongly influenced by the surface energies and roughness of the film surface *via* varying the molar mass of the constituent blocks.[31–33] To our knowledge, the surface-initiated atom transfer radical polymerization (SI-ATRP) of fluorinated chains grafted onto silica surface has never been described in the literature.

In this article, the synthesis and properties of the silica grafting diblock fluoroacrylate copolymer hybrids SiO_2-*g*-PMMA-*b*-P12FMA are reported. The synthesis was performed in two steps: (i) the preparation of monolayer SiO_2-initiator by the reaction of fumed silica particles with hydrosilylated undec-10-enyl, 2-bromo-2-methyl propionate. (ii) the SI-ATRP synthesis of poly(methylmethacrylate) (PMMA) and poly(dodecafluoroheptyl methacrylate) (P12FMA) to obtain silica grafted diblock copolymer hybrid SiO_2-*g*-PMMA-*b*-P12FMA in the mass ratio of SiO_2-initiator/MMA/12FMA = 1/72.50/18.15, 1/72.50/45.38 and 1/181.26/18.15. Meanwhile, for comparison, the conventional initiator of ethyl 2-bromoisobutyrate (EBiB) was also used to produce the diblock copolymers E-PMMA-*b*-P12FMA in this paper. Their chemical structures were characterized by ^{1}H NMR, ^{19}F NMR spectroscopy and size exclusion chromatography-multiangle laser light scattering (SEC-MALLS). The obtained SiO_2-*g*-PMMA-*b*-P12FMA hybrids were observed by transmission electron microscopy (TEM). The surface properties of the films were investigated by static contact angle (SCA) and dynamic contact angle (DCA) measurements, atomic force microscope (AFM) and X-ray photoelectron spectroscopy (XPS). The water absorption of the film was monitored by the quartz crystal microbalance with dissipation (QCM-D). The thermostablity was further analyzed by thermo gravimetric analysis (TGA). Meanwhile, the results for SiO_2-*g*-PMMA-*b*-P12FMA and E-PMMA-*b*-P12FMA were compared.

2. Experimental

2.1 Materials

Fumed silica (VK-SP15) with an average diameter of 10–25 nm and a specific area of 230 m^2 g^{-1} was supplied by the Hang Zhou New Material Company of China. Dodecafluoroheptyl methacrylate ($C_{11}H_8O_2F_{12}$, 12FMA, liquid) was supplied by XEOGIA Fluorine-Silicon Chemical Co. Ltd. (China). Methyl methacrylate (MMA, 99% wt, Aldrich) was purified by extraction with 5% aqueous sodium hydroxide and distilled from calcium hydride prior to use. Triethylamine was purified by distillation. Karstedt catalyst (platinum–divinyltetramethyldisiloxane complex), undecylenyl alcohol (10-undecen-1-ol, $C_{11}H_{22}O$), 2-bromo-2-methylpropionyl bromide (BMPB), methylene chloride, chloroform, dichloromethylsilane (DCMS), tetrahydrofuran (THF), *N*,*N*,*N*9,*N*9,*N*0-pentamethyldiethylenetriamine (PMDETA), copper(I) bromide and 2-bromoisobutyrylbromide (BiBB) were used as received. *N*,*N*-Dimethylformamide (DMF) was stirred over CaH_2 for 12 h at room temperature, and then distilled under reduced pressure prior to use.

2.2 Synthesis of silica surface-initiator

The first step was the synthesis of undec-10-enyl, 2-bromo-2-methyl propionate. 6.0 ml 10-undecen-1-ol (29.60 mmol), 20.0 ml dry methylene chloride and 7.0 ml triethylamine (50.22 mmol) were added to a 100 ml Schlenk flask. Then, 4.0 ml BMPB (32.36 mmol) was added dropwise at 0 °C. The reaction was carried out under nitrogen protection at 0 °C for 2 h and then at room temperature for 24 h. The crude product was isolated by filtration and extraction using an aqueous-saturated ammonium chloride solution. The obtained undec-10-enyl, 2-bromo-2-methyl propionate was then distilled at 55 °C under reduced pressure (6–7 mmHg) (yield: 75%).

The second step was the hydrosilylation of undec-10-enyl, 2-bromo-2-methyl propionate. A mixture of 1.2 ml undec-10-enyl, 2-bromo-2-methyl propionate (6.27 mmol), 60 μl Karstedt's catalyst and 9.0 ml DCMS (86.06 mmol) was added to a 100 ml dried Schlenk flask, and was allowed to react in the dark for 24 h at 40 °C under nitrogen protection. The catalyst was removed by quickly filtering the product through a short plug of dry silica, and the excess DCMS was removed under reduced pressure. Then, the product was used directly for the silanization step to obtain hydrosilylated undec-10-enyl, 2-bromo-2-methyl propionate (purity: 90%).

The last step was the synthesis of silica surface-initiator (SiO_2-initiator). Silica particles were dried in vacuum at 110 °C for 6–7 h and were dispersed in dry THF by ultrasonication. 15 ml silica particle solution in THF was added to a 200 ml dried Schlenk flask. Then, 0.25 g hydrosilylated undec-10-enyl, 2-bromo-2-methyl propionate (0.576 mmol) was introduced through a cannula, followed by the dropwise addition of 1.25 ml triethylamine (8.97 mmol). The reaction was carried out under N_2 atmosphere at 40 °C for 40 h. The particles were isolated by centrifugation and purified by Soxhlet extraction exposed to refluxing 50/50 (v/v) methylene chloride/diethyl ether for 8 h. The purified particles were redispersed in 10 ml of DMF. The solution was used as the silica initiator for ATRP. The synthesis scheme of the SiO_2-initiator is given in Scheme 1(I).

2.3 Synthesis of SiO_2-*g*-PMMA-*b*-P12FMA hybrids by SI-ATRP

The mixture of 0.4546 mmol CuCl, 0.0358 mmol $CuCl_2$, 32.96 mmol MMA and 0.4546 mmol PMDETA were added to a 100 ml dried Schlenk flask under N_2 atmosphere, which was sealed with a rubber septum prior to three vacuum/N_2 cycles. The mixture was stirred until a homogeneous medium formed. Then, 10 ml SiO_2-initiator (0.4546 mmol in DMF) was added to the flask by cannula transfer and the reaction mixture was

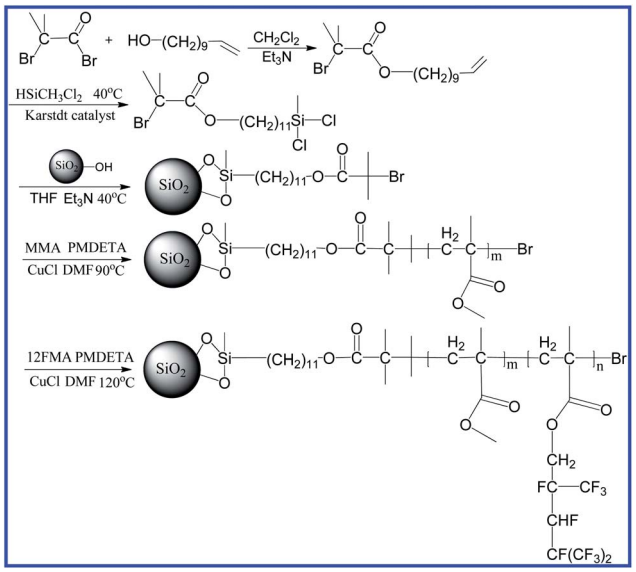

Scheme 1 Synthesis of the SiO_2-initiator (I) and SiO_2-*g*-PMMA-*b*-P12FMA (II).

heated to 90 °C and was kept for 12 h. In this case, the appearance of the reaction system varied from light green to turquoise blue, indicating a change in the nature of the copper complexes. Finally, 8.250 mmol 12FMA was added and was allowed to continue the reaction for 12 h. When the polymerization was stopped, THF was added to dilute the mixture, and the nanoparticles were isolated by centrifugation. The particles were repeatedly dispersed in THF, isolated by centrifugation to remove physically adsorbed polymers and the product SiO_2-*g*-PMMA-*b*-P12FMA was dried in a vacuum oven at 40 °C overnight. The conversion of MMA after 12 h reaction was 82% after 12 h reaction and the conversion of 12FMA after 12 h reaction was 35%. The detailed synthesis route for SiO_2-*g*-PMMA-*b*-P12FMA is given in Scheme 1(II). In this paper, three mass ratios of SiO_2–Br/MMA/12FMA = 1/72.50/18.15, 1/72.50/45.38 and 1/181.26/18.15 for sample S1, S2 and S3 were used to obtain SiO_2-*g*-PMMA-*b*-P12FMA hybrid particles, as shown in Table 1.

2.4 Synthesis of E-PMMA and E-PMMA-*b*-P12FMA with the EBiB initiator

In order to compare the differences of the SiO_2-initiator and normal initiator, EBiB was selected as the initiator, instead of the SiO_2-initiator to obtain E-PMMA-*b*-P12FMA (sample S4). The polymerization procedure was the same as for the SiO_2-initiator. The polymerization conditions and detailed values are listed in Table 1.

2.5 Characterization

Nuclear magnetic resonance (^{1}H NMR and ^{19}F NMR) spectroscopy was used to characterize the chemical structures of SiO_2-*g*-PMMA and SiO_2-*g*-PMMA-*b*-P12FMA by a BrukerAC500 NMR spectrometer using the solvent peak as reference ($CDCl_3$). The molecular weights and molecular weight distribution of the resultant copolymers were measured using a DAWN EOS size exclusion chromatography-multiangle laser light scattering (SEC-MALLS) instrument equipped with a viscometer (Wyatt Technology, USA) using the SEC/DAWN EOS/Optilab rEX/QELS model at 25 °C, after SiO_2-*g*-PMMA and SiO_2-*g*-PMMA-*b*-P12FMA were treated by HF to isolate SiO_2. DMF was used as the eluent at a flow rate of 0.5 ml min^{-1}. The individual particles of obtained SiO_2-*g*-PMMA-*b*-P12FMA hybrid were observed by transmission electron microscopy (TEM) with a JEM-3010 TEM at an acceleration voltage of 100 kV. Samples were prepared by drop-casting micelle in $CHCl_3$ solution onto carbon-coated copper grids, and then air-drying at room temperature before measurement.

The film was prepared by casting 10% wt homogeneous solution of SiO_2-*g*-PMMA-*b*-P12FMA in $CHCl_3$ on a glass slide and drying at ambient temperature for 72 h. The film properties were investigated by X-ray photoelectron spectroscopy (XPS), atomic force microscope (AFM), static contact angle (SCA), dynamic contact angle (DCA) and surface free energy. XPS measurements were processed on the air exposed film surface by an AXIS ULTRA (England, KRATOS ANALYTICAL Ltd) using an Al-Kα monochromatic X-ray source (1486.6 eV) operated at 150 W. The overview scans were obtained with a pass energy of 160 eV and acquisition time of 220 s. NT-MDT new Solver-Next was used to characterize the surface topographies and roughness (root-mean-square roughness) of the same film samples. The measurements were taken at room temperature under 38–42% R.H. Tip information: radius <10 nm, cantilever length 90 ± 5 mm; width 40 ± 3 mm; thickness 2.0 ± 0.5 mm, resonant frequency 330 kHz, force constant 48 N m^{-1}. SCA measurements for both the deionized water and hexadecane on the air-exposed film surfaces were performed on a JY-82 contact angle goniometer (Hebei Chengde Testing Machine Co. Ltd China) by the sessile drop method with a microsyringe at 25 °C. The instrument error is ±0.50°. An average of nine readings of contact angles was used as the final value for each sample (error

Table 1 Component values for the preparation of SiO_2-*g*-PMMA-*b*-12FMA and E-PMMA-*b*-12FMA

Samples	SiO_2–Br/MMA/12FMA (molar ratios)	SiO_2–Br (mmol)	EBiB (mmol)	MMA (mmol)	12FMA (mmol)	CuCl (mmol)	$CuCl_2$ (mmol)	PMDETA (mmol)	DMF (ml)
S1	1/72.50/18.15	0.4546	—	32.96	8.250	0.4546	0.0358	0.4546	15
S1	1/72.50/45.38	0.4546	—	32.96	20.63	0.4546	0.0358	0.4546	15
S3	1/181.26/18.15	0.4546	—	82.40	8.250	0.4546	0.0358	0.4546	15
S4	E-PMMA-P12FMA (1/77.92/22.0)	—	0.5127	39.95	10.00	0.5132	—	0.5132	15

about 2–3%). The surface free energies of the samples were evaluated by applying the Owens and Wendt method based on static contact angle values.

A quartz crystal microbalance with dissipation (QCM-D) monitoring (Q-Sense E1, Sweden) at 25 °C was performed to discuss the water adsorption and viscoelasticity of SiO_2-*g*-PMMA-*b*-P12FMA films. AT-cut piezoelectric quartz crystals covered with gold were used with a fundamental frequency of 5 MHz and a diameter of 14 mm. The film samples for the measurements were prepared by dropping 2 ml of the polymer solutions (5% wt, filtering through 0.45 μm disposable PA membrane) on the surfaces of quartz crystals and drying in a vacuum oven at 30 °C for 12 h. The Δf and ΔD were recorded at 15 MHz with air as the baseline.

The thermal stabilities of the SiO_2-*g*-PMMA-*b*-P12FMA hybrid particles were evaluated by thermo gravimetric analysis (TGA) performed under N_2 atmosphere with the rate of temperature rise 10 °C min^{-1} at a high temperature of 800 °C using TGA analyzer (STA449C Jupiter from NETZSCH).

3. Results and discussion

3.1 Synthesis of the SiO_2-*g*-PMMA-*b*-P12FMA hybrid

The procedures for the synthesis of the SiO_2-initiator and SiO_2-*g*-PMMA-*b*-P12FMA are shown in Scheme 2. The SiO_2-initiator was prepared by the hydrosilylation of undec-10-enyl, 2-bromo-2-methyl propionate (UBMP) and silica nanoparticles. The carbon–carbon double bonds of UBMP serve as the growth sites during the subsequent hydrosilylation with dichloromethylsilane (DCMS). This is confirmed in Fig. 1(I) for UBMP by δ 1.29 (2H, CH_2), 1.67 (2H, CH_2), 1.93 [6H, $(CH_3)_2$], 2.04 (2H, CH_2), 4.16 (2H, CH_2), 4.91–5.01 (2H, CH_2) and 5.80 (1H, CH), and in Fig. 1(II) for hydrosilylated UBMP by δ 0.50 [3H, CH_3], 0.86 (2H, CH_2), 1.28–1.31 [18H, $(CH_2)_8$], 1.68 (2H, CH_2), 1.92 [6H, $(CH_3)_2$] and 4.17 (2H, CH_2).

The end groups of $-SiCH_3Cl_2$ in hydrosilylated undec-10-enyl, 2-bromo-2-methyl propionate formed chemical bonds with the –OH groups on the surface of silica particles to obtain a monolayer of the anchored silica particles ATRP-initiator (SiO_2-initiator). The FTIR spectrum for the SiO_2-initiator (ESI, S1†) shows the absorption at 2983 and 2899 cm^{-1} due to the alkyl C–H stretching vibration, but these absorptions are non-existent in the SiO_2 particles, which indicates that the initiator has been

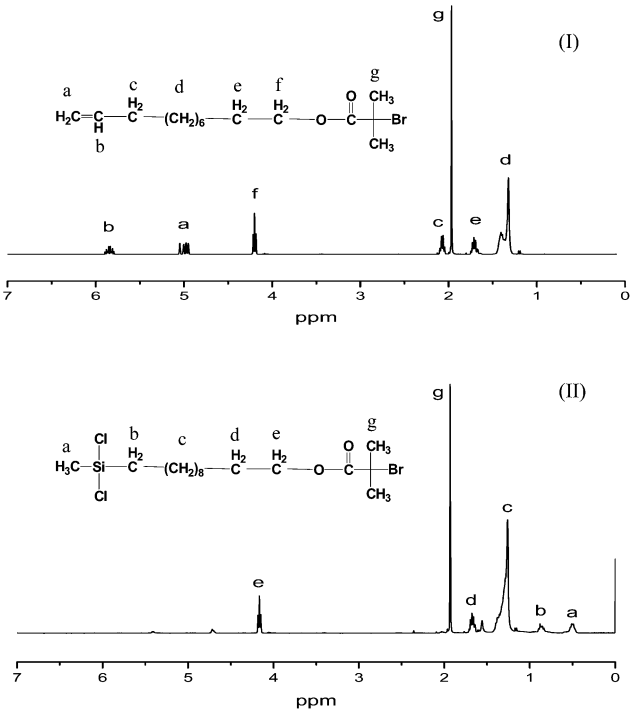

Fig. 1 ^{1}H NMR spectra of undec-10-enyl, 2-bromo-2-methyl propionate (I) and the hydrosilylated undec-10-enyl, 2-bromo-2-methyl propionate (II).

polymerized onto the SiO_2 particle's surface of the SiO_2-initiator. Furthermore, the TGA curves (ESI, S2†) indicate that the weight retention at 800 °C is 99.7% for SiO_2 particles due to the water loss, but the initiator particles have 78.9% weight retention. If the mass percentage of the residue at 800 °C is used as the reference, the weight increase of SiO_2-initiator particles relative to that of SiO_2 would be 20.8%. Therefore, the density of the SiO_2-initiator is 0.573 mmol per gram SiO_2-initiator. Furthermore, the density of Br on the SiO_2 surface is calculated as 0.05% (*i.e.* 0.625 mmol per gram SiO_2-initiator) from the XPS data of SiO_2–Br (Fig. 5a).

SiO_2-*g*-PMMA-*b*-P12FMA hybrids were obtained by the SI-ATRP of PMMA-*b*-P12FMA shell on the surface of the silica core. The ^{1}H NMR spectrum of SiO_2-*g*-PMMA (Fig. 2I), SiO_2-*g*-PMMA-*b*-P12FMA (Fig. 2II) and ^{19}F-NMR spectrum of SiO_2-*g*-PMMA-*b*-P12FMA (Fig. 2III) reveal the characteristic signals at δ 0.841 &

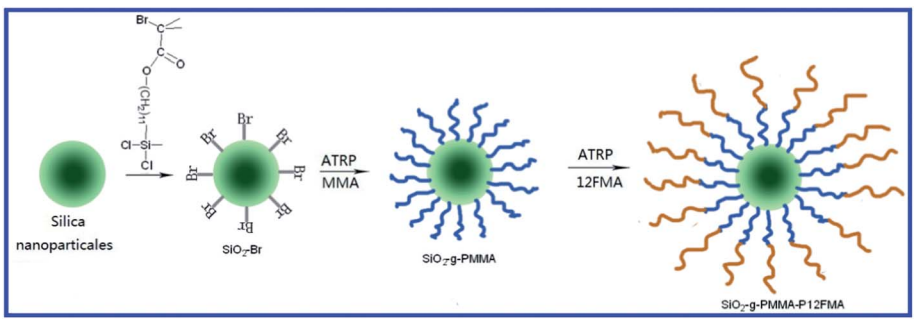

Scheme 2 Formation of the SiO_2-*g*-PMMA-*b*-P12FMA hybrids.

1.020 ppm, 1.832–1.960 ppm and 3.600 ppm in Fig. 2I for the PMMA segment, the signals at 4.456 ppm and 5.513 ppm in Fig. 2II for the P12FMA segment, and fluorine multiple peak signals in the ^{19}F-NMR in Fig. 2III for P12FMA. These results indicate that SiO_2-*g*-PMMA-*b*-P12FMA was successfully prepared by SI-ATRP.

The SEC-MALLS results of the SiO_2-*g*-PMMA and SiO_2-*g*-PMMA-*b*-P12FMA are given in Fig. 3 and Table 2. PMMA and E-PMMA-*b*-P12FMA (E/MMA/12FMA = 1/77.92/22.00) are used for comparison in order to confirm the controlled radical polymerization of the SI-ATRP approach. Fig. 3a shows that the molecular weights were 7558.7 g mol^{-1}, 17 810.75 g mol^{-1} and 7786.67 g mol^{-1} for PMMA (1/72.5), PMMA (1/181.26) and E-PMMA (1/77.92), respectively. For the two initiators to obtain diblock copolymers, the polydispersity index (PDI) of 1.12–1.25 in Fig. 3b reveals a narrow distribution of molecular weight, which illustrates that the polymerization initiated both by SiO_2-initiator and EBIB are typically controllable ATRP. The monomodal molecular weight distributions in Fig. 3b are 11 700, 18 000, 21 300 g mol^{-1} for SiO_2-*g*-PMMA-*b*-P12FMA (SiO_2/MMA/12FMA = 1/72.50/18.15, 1/72.50/45.38 and 1/181.26/18.15), respectively. Table 2 indicates that the obtained M_n is lower than the theoretical value for all the samples, and that M_n for E-PMMA-P12FMA (13 500 g mol^{-1}) is higher than SiO_2-*g*-PMMA-P12FMA (1/72.50/18.15) (11 700 g mol^{-1}), which shows the lower activity of the SiO_2-initiator. All the results from the ^{1}H-NMR, ^{19}F-NMR and SEC-MALLS confirm that the synthesis of SiO_2-*g*-PMMA-P12FMA proceeded as Table 1 for the monomer feed ratios, reactant concentrations, reaction conditions employed and synthetic routes as expected.

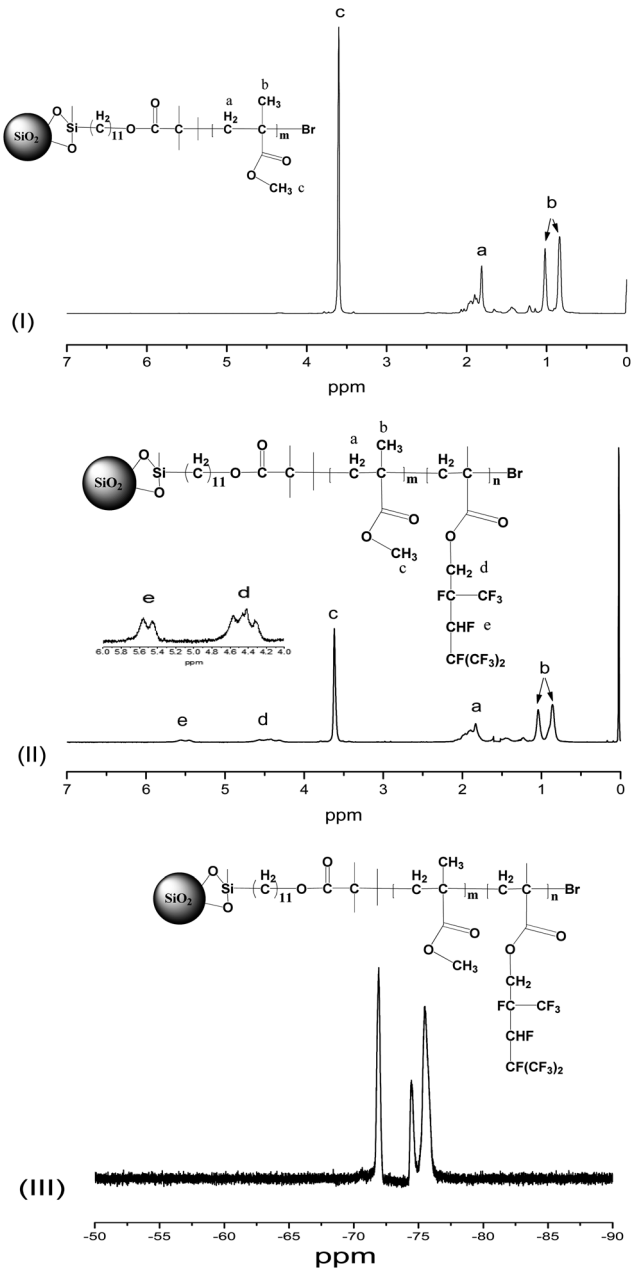

Fig. 2 ^{1}H-NMR spectra of the SiO_2-*g*-PMMA (I), SiO_2-*g*-PMMA-*b*-P12FMA (II), and ^{19}F-NMR spectrum of the SiO_2-*g*-PMMA-*b*-P12FMA (III).

3.2 The particles of SiO_2-*g*-PMMA-*b*-P12FMA in $CHCl_3$ solution

It is known that the self-assembled aggregates formed by block copolymers strongly depend on the composition of the segments. Herein, the influence of different SiO_2/PMMA/P12FMA mass ratios as 1/72.50/18.15, 1/72.50/45.38 and 1/181.26/18.15 on the morphology of SiO_2-*g*-PMMA-*b*-P12FMA aggregates in $CHCl_3$ solution is explored by TEM (Fig. 4), based on the different solubilities of the segment PMMA (good) and the segment P12FMA (poor) in $CHCl_3$ solution. In order to better understand the morphology of SiO_2-*g*-PMMA-*b*-P12FMA particles, the particles of E-PMMA-*b*-P12FMA in $CHCl_3$ solution were used for comparison (Fig. 4a). E-PMMA-*b*-P12FMA could produce about 100–150 nm spherical particles composed of the dark core and the light shell observed. As the unsolvable chains in $CHCl_3$ solution could aggregate into the harder cores and the solvable chains into the shells of the micelles or vesicles,[32] the inner dark core should be formed by P12FMA, and the outer light shell should be formed by PMMA. However, for the morphology of the three SiO_2-*g*-PMMA-*b*-P12FMA samples, 25–30 nm core–shell spherical particles composed of the dark core and the light shell are observed in Fig. 4b–d by the particle shells densely twining together as the agglomerated particles. Comparatively, the relatively fewer PMMA and P12FMA segments in S1 (1/72.50/18.15) makes the particles arrange closely (Fig. 4b), the poor solubility of P12FMA segment enables S2 (1/72.50/45.38) to form congested aggregates (Fig. 4c), but the higher content of PMMA segment in S3 (1/181.26/18.15) leads to the formation of uniformly distributed particles and less agglomeration (Fig. 4d) attributed to the sufficient solubility of PMMA in $CHCl_3$ solution. It can also be found that the size of the SiO_2-*g*-PMMA-*b*-P12FMA hybrids (25–30 nm) are much smaller than the E-PMMA-*b*-P12FMA particles (100–150 nm), indicating that SiO_2 has been grafted by the dense PMMA-*b*-P12FMA *via* the SI-ATRP approach.

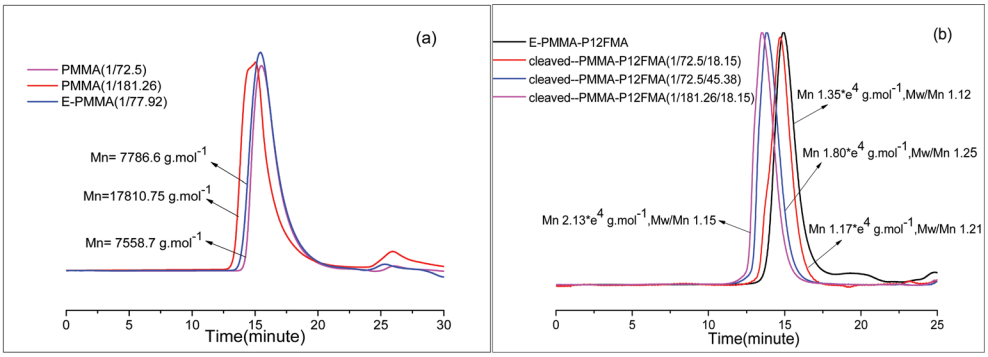

Fig. 3 GPC curves of (a) PMMA, and (b) diblock copolymer of E-PMMA-P12FMA (S4), the PMMA-*b*-P12FMA cleaved from SiO_2-*g*-PMMA-*b*-P12FMA in S1 (1/72.50/18.15), S2 (1/72.50/45.38) and S3 (1/181.26/18.15).

3.3 The surface composition, morphology and wettability of the SiO_2-*g*-PMMA-*b*-P12FMA films

These aggregates are expected to influence the surface composition, morphology, and therefore the resulting hydrophobic character of the films. The chemical compositions on the film top surface were analyzed by XPS in Fig. 5. The SiO_2-initiator (Fig. 5a) and E-PMMA-*b*-P12FMA were used for comparison (Fig. 5e). In Fig. 5a, the electron binding energy of O1s, C1s, Si2p and Br3d at 530.1 eV, 283.0 eV, 101.2 eV and 68.6 eV, respectively, indicate that the SiO_2-initiator has been successfully prepared. For the XPS spectrum of the SiO_2-*g*-PMMA-*b*-P12FMA films of S1 (Fig. 5b, 1/72.50/18.15), S2 (Fig. 5c, 1/72.50/45.38) and S3 (Fig. 5d, 1/181.26/18.15), the films are mainly composed of the elements F, O, C and Si, but the peak of Si is much weaker. Comparing with the stronger characteristic signal of the F element in E-PMMA-*b*-P12FMA Fig. 5e, b(S1) and c(S2) show less characteristic signals than Fig. 5e, but stronger signals than Fig. 5d(S3). This has been proven by the chemical composition in Table 3. The migration of P12FMA segments onto the film surface leads to the higher fluorine content of S1 (26.67%) and S2 (26.96%) because of the higher contribution of the P12FMA segments, but the lower fluorine content of S3 (18.21%) due to the lower P12FMA content.

The surface morphology of the SiO_2-*g*-PMMA-*b*-P12FMA films cast from $CHCl_3$ solution was investigated by AFM for the surface roughness (Fig. 6). Compared with the compact smooth surface of 30 nm root mean square roughness for E-PMMA-*b*-P12FMA film (Fig. 6a), three SiO_2-*g*-PMMA-*b*-P12FMA films were distributed with nanoscale particle agglomerates. Island type structures as 250 nm root mean square roughness are formed on the film surface of S1 (Fig. 6b, 1/72.50/18.15), the obvious honeycomb structure as 1–2 μm domains as a root mean square roughness of 500 nm is observed on the surface of S2 (Fig. 6c, 1/72.50/45.38), but a few individual heaves (the lighter points) as domains of approximately 40–60 nm height are scattered on the film surface of S3 to form 50 nm root mean square roughness (Fig. 6d, 1/181.26/18.15).

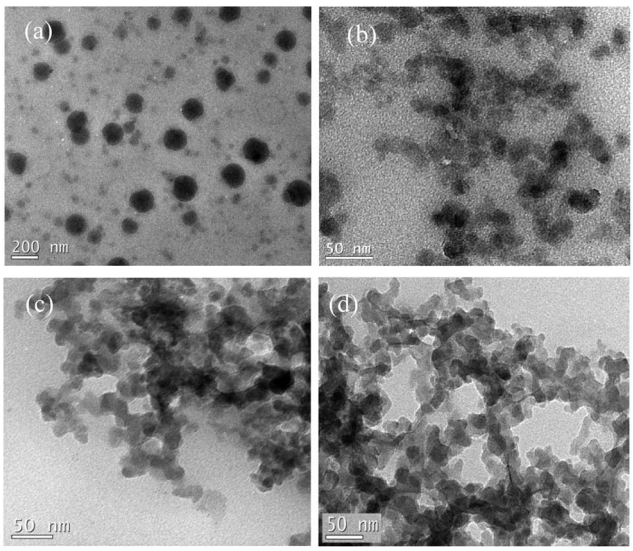

Fig. 4 TEM images for E-PMMA-*b*-P12FMA (a, S4) and SiO_2-*g*-PMMA-*b*-P12FMA for S1 (b, 1/72.50/18.15), S2 (c, 1/72.50/45.38) and S3 (d, 1/181.26/18.15) in $CHCl_3$ solution.

Actually, this composition and roughness will contribute much to the surface wettability, as shown in Table 3 evaluated by the static contact angles (SCAs) measurements for water and cetane, and the calculated surface free energy (γ_S). The SCAs indicate that the three film surfaces are not only sufficiently

Table 2 GPC characterization of PMMA-*b*-P12FMA cleaved from the SiO_2 surface

Sample	M_w/M_n	M_n ($\times 10^4$) g mol^{-1}	M_w ($\times 10^4$) g mol^{-1}	M_n ($\times 10^4$)(theo) g mol^{-1}
S1 (1/72.50/18.15)	1.21	1.17	1.42	1.49
S2 (1/72.50/45.38)	1.25	1.80	2.25	2.58
S3 (1/181.26/18.15)	1.15	2.13	2.45	2.58
S4 (1/77.92/22.00)	1.12	1.35	1.51	1.57

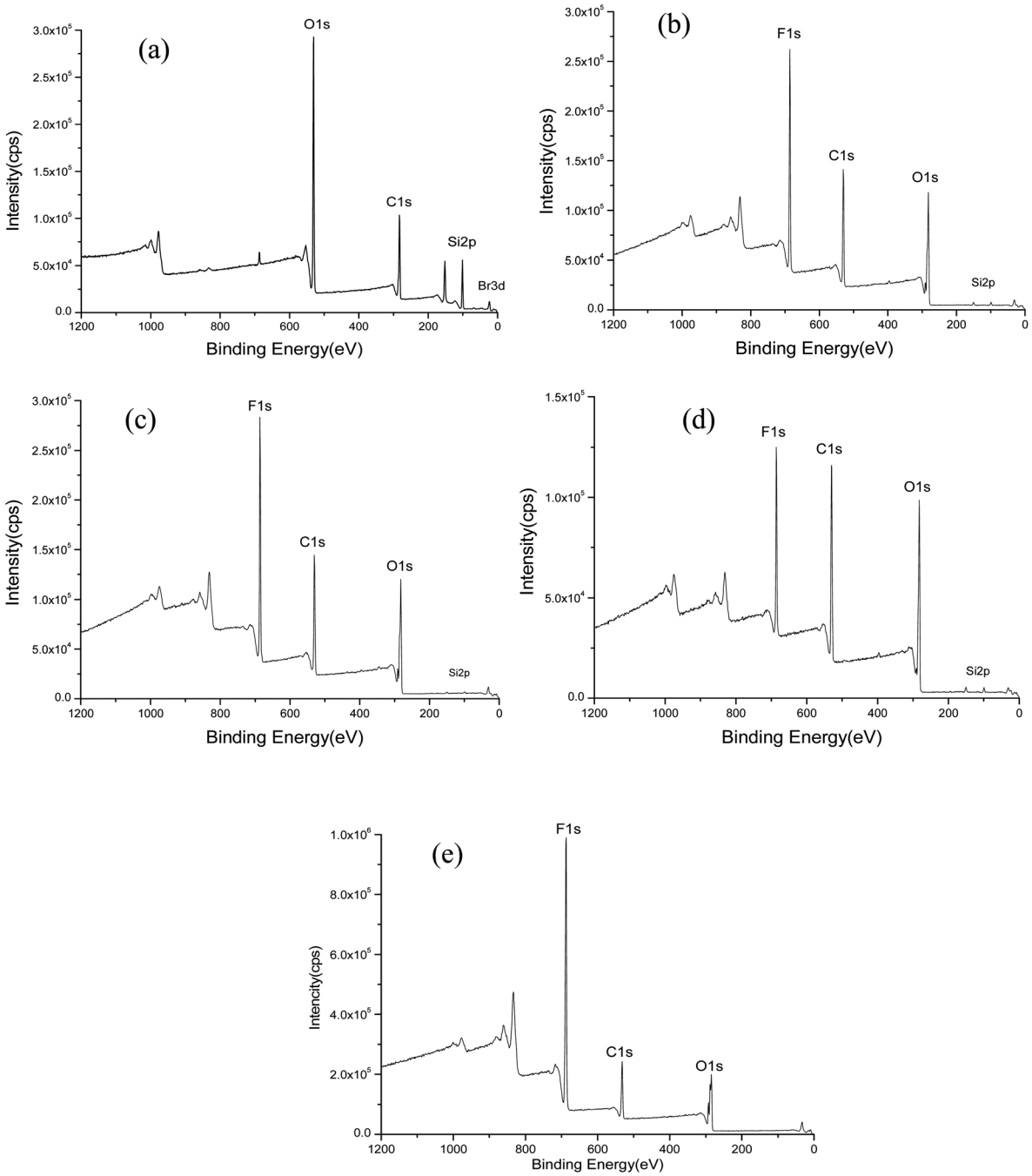

Fig. 5 XPS scanning spectrum for the powder of SiO_2–Br (a), the air-side surface of SiO_2-*g*-PMMA-*b*-P12FMA for S1 (b, 1/72.50/18.15), S2 (c, 1/72.50/45.38) and S3 (d, 1/181.26/18.15) and E-PMMA-*b*-P12FMA (e, S4).

hydrophobic (112–118°) compared with the S4 film (108°), but also that the S1 and S2 film are more oleophobic (73–78°) than the S4 film (56°). The obviously higher SCAs could lead to the lower surface energy for S1 and S2 (12.46 mN m^{-1} and 10.97 mN m^{-1}) than the E-PMMA-*b*-P12FMA film (17.48 mN m^{-1}), contributed to by the higher F content on the top surface and higher surface roughness. Although S3 is less oleophobic (45°) than others, it is the most hydrophobic (118°), and gets the highest surface energy (22.33 mN m^{-1}) due to the lower fluorine content of S3 (18.21%). Compared with S1 and S4, the results also suggest that the grafting of fluorinated copolymers onto silica nanoparticles could obtain, not only the oleophobic property of film surface, but also an increase in the hydrophobicity of such films, and thus the lower surface free energy. Additionally, the dynamic contact angle (DCA) measurements of water (WCA) and cetane (CCA) for the films are measured in Table 3. The surface of the S3 film obtains the highest θ_a (114°) and θ_r (106°) for WCA, but the lowest θ_a (44°) and θ_r (38°) for CCA, and the biggest θ_h of WCA and HAC (6°) among the three hybrids, revealing that increasing the PMMA content favors a

Table 3 Contact angles, surface free energy, and chemical compositions of the films[a]

Sample	θ_{H_2O}/°	θ_{cetane}/°	γ_S/mN m^{-1}	Element content/% wt			
				F	Si	C	O
SiO_2–Br	—	—	—	—	65.54	16.94	17.47
S1 (1/72.50/18.15)	112 (110 106, 4)*	73 (72, 67, 5)*	12.46	26.67	1.34	53.84	18.15
S2 (1/72.50/45.38)	114 (112 108, 4)	78 (74,70, 4)	10.97	26.96	0.63	54.21	18.20
S3 (1/181.26/18.15)	118 (114 108, 6)	45 (44,38, 6)	22.33	18.21	1.56	58.87	20.98
S4 (1/77.92/22.0)	108 (105, 97, 8)	56 (52,44, 8)	17.48	23.87	—	55.68	20.45

[a] Where, * the numbers in brackets refer to the advancing angle (θ_a), receding angle (θ_r) and hysteresis angle ($\theta_h = \theta_a - \theta_r$), respectively.

higher contact angle hysteresis, and therefore better hydrophobic, but less oleophobic properties than increasing the P12FMA content in S2. The highest θ_h of WCA and HAC for the S4 film (8° for WCA and HCA) indicates that the SiO_2 involved in the copolymer is favourable for obtaining lower contact angle hysteresis.

Furthermore, in order to understand the surface water adsorption of E-PMMA-P12FMA and SiO_2-*g*-PMMA-P12FMA films casting from $CHCl_3$ solutions, the water adsorption curves investigated by QCM-D are obtained in Fig. 7. The Δf in the adsorption curves is used to indicate the adsorbed amounts of probe liquids and the ΔD is used to evaluate the viscoelasticity of the adsorbed layer. In Fig. 7a for E-PMMA-P12FMA (S4) and Fig. 7d for S3 (1/181.26/18.15) with fewer P12FMA segments, similar absorption curves are observed. When water is absorbed on the surface of films, Δf and ΔD quickly reach the adsorption equilibrium, showing the fluoride side chains are vertically distributed on the surface for a relatively ordered structure, so that the adsorbed water forms a relatively loose adsorption layer on the film surface. This process is suggested in the adsorption model of Fig. 7I. In order to explain the fluorine-containing groups migrating onto the film surface during the film formation, the fluorinated brush segment upon contact with water is placed further towards the Si-particle surface, and the PMMA region is placed closer to the Si-particle surface in the adsorption model of Fig. 7. The adsorbed amount of water and the viscoelasticity of the adsorbed layer for both of them at the end of absorption are similar ($\Delta f = 450$, $\Delta D = 130$ and 170) due to the similar fluorine content (26.67% and 23.87%). For S1 (1/72.50/18.15) with the same PMMA and P12FMA segments in Fig. 7b, SiO_2 plays a role of supporting the copolymer chains in the film, but fluorine-containing chains are migrating onto the

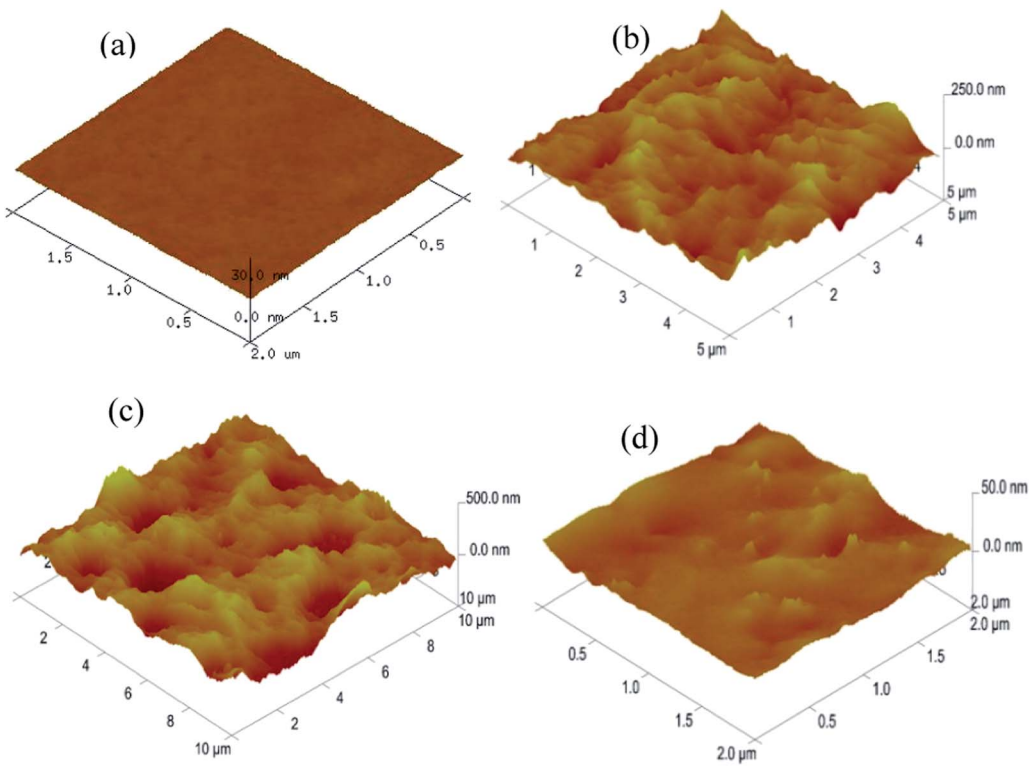

Fig. 6 AFM images of E-PMMA-P12FMA (a, S4) and SiO_2-*g*-PMMA-*b*-P12FMA for S1 (b, 1/72.50/18.15), S2 (c, 1/72.50/45.38) and S3 (d, 1/181.26/18.15).

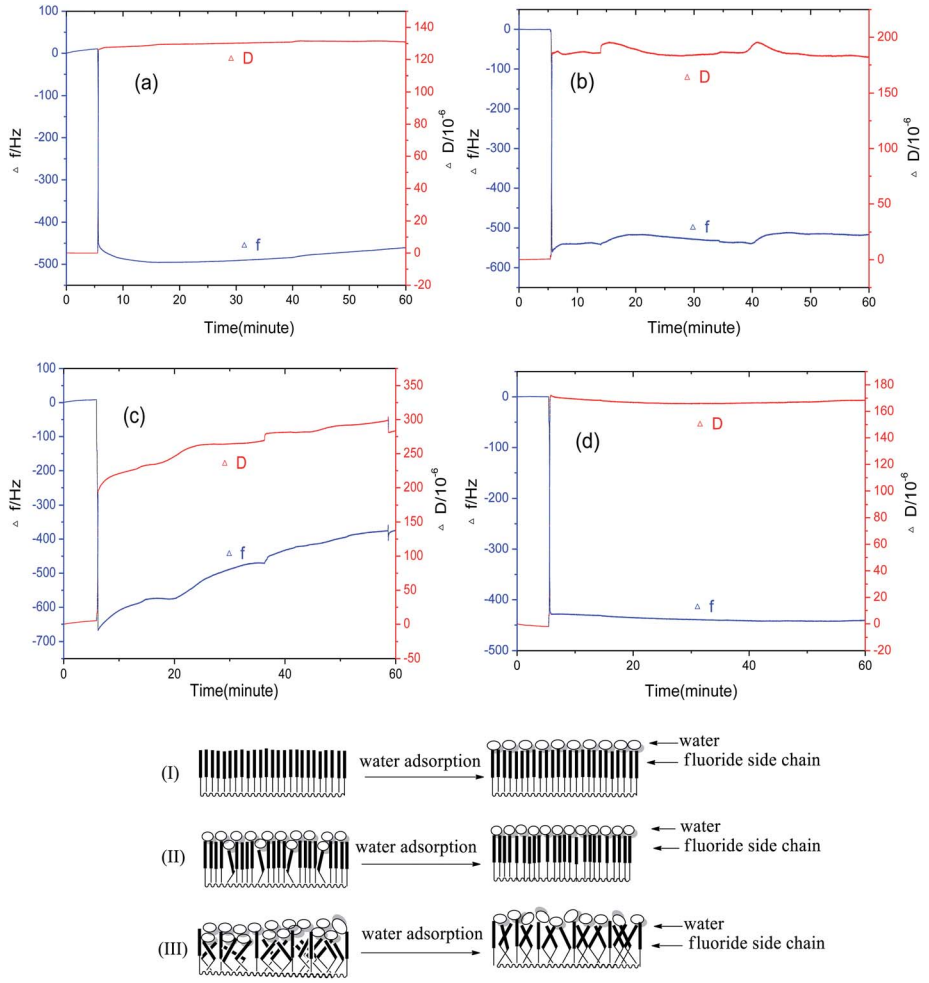

Fig. 7 Frequency (Δf) and dissipation changes (ΔD) for water by QCM-D measurements for E-PMMA-P12FMA (S4) and SiO_2-*g*-PMMA-*b*-P12FMA for S1 (1/72.50/18.15), S2 (1/72.50/45.38), S3 (1/181.26/18.15), and water adsorption models on the film surface (I–III).

film surface, which will lead to the fluoride side chains forming a disordered structure Fig. 7(II). With water flowing over the film surface, the disordered structure transforms to an ordered structure and the adsorbed water begins to leave the surface, which causes a small increase in the Δf and ΔD, but finally reaches the adsorption equilibrium at $\Delta f = 550$ and $\Delta D = 180$, showing high amounts of adsorbed water and a higher viscoelasticity of the adsorbed layer than S4 and S3. However, for the SiO_2-*g*-PMMA-*b*-P12FMA of S2 (1/72.50/45.38), a very different adsorption behavior is observed (Fig. 7c). Many more P12FMA segments make the fluorine-containing chains migrate intensively crowdedly and finally form a rather rough surface (Fig. 6c). Therefore, when water is flowing continually over this film surface, the ΔD increases with the increases of Δf, indicating that a relatively ordered and loosely absorbed structure is formed in Fig. 7(III) with the highest viscoelasticity of $\Delta D = 268$.

3.4 The thermostability of the SiO_2-*g*-PMMA-*b*-P12FMA hybrid

The thermostabilities of the E-PMMA-P12FMA and SiO_2-*g*-PMMA-*b*-P12FMA hybrids were evaluated by TGA (Fig. 8). E-PMMA-P12FMA in Fig. 8a shows the starting degradation at 250 °C. But S1 (Fig. 8b, 1/72.50/18.15) and S2 (Fig. 8c, 1/72.50/45.38) gave similar decomposition temperatures at 320 °C with the weight losses of 85.7% wt and 85.9% wt, respectively. For S3, a decomposition temperature at 280 °C with the weight loss of 83.2% wt has a slightly lower thermostability than S1 and S2. These results indicate that a higher PMMA content in S3 will result in the reduction of the decomposition temperature, but increasing the P12FMA content in SiO_2-*g*-PMMA-*b*-P12FMA from S1 to S2 could not obviously improve the thermostability. Furthermore, the end decomposition temperatures are observed at 430 °C for S1 and S2, and 410 °C for S3. Therefore, in the case of the "grafting from" polymerization of SI-ATRP, the thermostabilities of SiO_2-*g*-PMMA-*b*-P12FMA hybrids are much higher than E-PMMA-P12FMA, and the higher content of the 12FMA segment in SiO_2-*g*-PMMA-*b*-P12FMA (1/72.50/45.38) could provide the higher end decomposition temperatures due to the thermostabilities of the P12FMA segments. This was also proven by Nelly Durand[9] *et al.* in their research that silica nanoparticles activated with vinyl groups show an onset decomposition temperature around 300 °C, but silica modified with "grafting from" polymerization exhibits

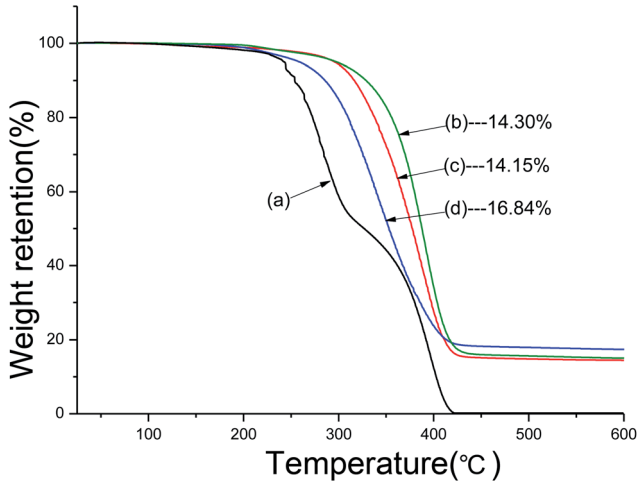

Fig. 8 TGA diagram of S4 (a) and SiO_2-*g*-PMMA-*b*-P12FMA for S1 (1/72.50/18.15) (b), S2 (1/72.50/45.38) (c), S3 (1/181.26/18.15) (d).

around an onset decomposition temperature of 430 °C attributed to the PVDF grafted chains. All of these results demonstrate the good compatibility between SiO_2, PMMA and P12FMA.

4. Conclusion

The grafting of PMMA-*b*-P12FMA chains onto the silica surface was used to prepare the SiO_2-*g*-PMMA-*b*-P12FMA hybrid by a successful "grafting from" SI-ATRP technique. 25–30 nm spherical core–shell particles were obtained for three SiO_2-*g*-PMMA-*b*-P12FMA hybrids with the mass ratios of SiO_2/PMMA/P12FMA = 1/72.50/18.15, 1/72.50/45.38 and 1/181.26/18.15. Compared with the compact smooth surface for E-PMMA-*b*-P12FMA obtained by EBiB initiator, the three SiO_2-*g*-PMMA-*b*-P12FMA films have nanoscale particle agglomerates distributed and a higher surface roughness. The migration of P12FMA segments onto the film surface will lead to the higher fluorine content for S1 (26.67%) and S2 (26.96%). The grafting of fluorinated copolymers onto silica nanoparticles could obtain a lower contact angle hysteresis. A much higher P12FMA content makes the fluoride side chains migrate and finally form a rather rough surface. Actually, this roughness and composition could provide three film surfaces with sufficient hydrophobicity (112–118°) compared with the E-PMMA-*b*-P12FMA film (108°), and sufficient oleophobicity (73–78°) for S1 and S2 than the E-PMMA-*b*-P12FMA film (56°). The surface of the S3 film obtains the highest θ_a (114°) and θ_r (106°) for WCA, but the lowest θ_a (44°) and θ_r (38°) for CCA, and the biggest θ_h of WCA and HAC (6°) among the three hybrids, revealing that increasing the PMMA content is favorable for higher contact angle hysteresis, and therefore has better hydrophobicity but less oleophobic properties than increasing the P12FMA content in S2. Finally, the SiO_2-*g*-PMMA-*b*-P12FMA hybrid shows higher thermostabilities for the thermal decomposition temperature at 450 °C. Such a hybrid is recommended as a possible coating material.

Acknowledgements

This work has been financially supported by the National Natural Science Foundation of China (NSFC Grants no. 51373133 and 51073126), by the National Basic Research Program of China (973 Program, no. 2012CB720904), and by the State Administration of Cultural Heritage (20110128). The authors also wish to express their gratitude for the MOE Key Laboratory for Non-equilibrium Condensed Matter and Quantum Engineering of Xi'an Jiaotong University.

References

1 W. Timothy and E. P. Timothy, *J. Am. Chem. Soc.*, 2001, **123**, 7497.
2 D. J. Li, X. Sheng and B. Zhao, *J. Am. Chem. Soc.*, 2005, **127**, 6248.
3 T. Wu, Y. F. Zhang, X. F. Wang and S. Y. Liu, *Chem. Mater.*, 2008, **20**, 101.
4 Y. Yang, X. H. Yan, Y. Cui, Q. He, D. X. Li, A. H. Wang, J. B. Fei and J. B. Li, *J. Mater. Chem.*, 2008, **18**, 5731.
5 Y. H. Hu, C. Y. Chen and C. C. Wang, *Polym. Degrad. Stab.*, 2004, **84**, 545.
6 G. Carrot, S. M. Scholz, C. J. Plummer, J. L. Hedrick and J. G. Hilborn, *Chem. Mater.*, 1999, **11**, 3571.
7 L. Zhu and B. Zhao, *J. Phys. Chem. B*, 2008, **112**, 11529.
8 N. Durand, B. Boutevin, G. Silly and B. Ameduri, *Macromolecules*, 2011, **44**, 8487.
9 N. Durand, P. Gaveau, G. Silly, B. Ameduri and B. Boutevin, *Macromolecules*, 2011, **44**, 6249.
10 R. Bindushree, R. Rajesh and J. B. William, *Soft Matter*, 2006, **2**, 386.
11 C. Perruchot, M. A. Khan, A. Kamitsi and S. P. Armes, *Langmuir*, 2001, **17**, 4479.
12 R. Barbey, L. Lavanant, D. Paripovic, N. Schuwer, C. Sugnaux, St. Tugulu and H. A. Klok, *Chem. Rev.*, 2009, **109**, 5437.
13 G. Chang, L. He, W. Zheng, A. Z. Pan, J. Liu, Y. J. Li and R. J. Cao, *J. Colloid Interface Sci.*, 2013, **396**, 129.
14 Y. X. Li, Z. Q. Wang, H. Gu and G. Xue, *J. Colloid Interface Sci.*, 2011, **355**, 269.
15 F. J. Xu, J. P. Zhao, E. T. Kang and K. G. Neoh, *Ind. Eng. Chem. Res.*, 2007, **46**, 4866.
16 O. Prucker and J. Ruhe, *Macromolecules*, 1998, **31**, 602.
17 M. Mullner, J. Y. Yuan, S. Weiss, A. Walther, M. Fortsch, M. Drechsler and A. H. E. Muller, *J. Am. Chem. Soc.*, 2010, **132**, 16587.
18 C. E. Soto, S. S. Turksen, J. H. Qiu, Z. Zhou and P. S. Russo, *Langmuir*, 2010, **26**, 15604.
19 H. L. Wang, K. Schaefer, A. Pich and M. Moeller, *Chem. Mater.*, 2011, **23**, 4748.
20 N. Durand, P. Gaveau, G. Silly, B. Ameduri and B. Boutevin, *Macromolecules*, 2011, **44**, 6249.
21 K. Matyjaszewski and J. H. Xia, *Chem. Rev.*, 2001, **101**, 2921.
22 C. J. Hawker, A. W. Bosman and E. Harth, *Chem. Rev.*, 2001, **101**, 3661.
23 L. Bombalski, K. Min, H. C. Dong, C. B. Tang and K. Matyjaszewski, *Macromolecules*, 2007, **40**, 7429.

24 T. Morinaga, M. Ohkura, K. Ohno, Y. Tsujii and T. Fukuda, *Macromolecules*, 2007, **40**, 1159.
25 B. J. Privett, J. Youn, S. A. Hong, J. Lee, J. Han, J. Shin and M. H. Schoenfisch, *Langmuir*, 2011, **27**, 9597.
26 Y. Koda, T. Terashima, A. Nomura, M. Ouchi and M. Sawamoto, *Macromolecules*, 2011, **44**, 4574.
27 R. Campos, A. J. Guenthner, T. S. Haddad and J. M. Mabry, *Langmuir*, 2011, **27**, 10206.
28 N. Durand, D. Mariot, B. Ameduri, B. Boutevin and F. Ganachaud, *Langmuir*, 2011, **27**, 4057.
29 M. D. Rodwogin, C. S. Spanjers, C. Leighton and M. A. Hillmyer, *Nano*, 2010, **4**, 725.
30 K. Y. Mya, E. M. J. Lin, C. S. Gudipati, H. B. A. S. Gose and C. B. He, *J. Phys. Chem. B*, 2010, **114**, 9128.
31 M. A. Raza, E. S. Kooij, A. Silfhout and B. Poelsema, *Langmuir*, 2010, **26**, 12962.
32 A. Olivier, F. Meyer, J. M. Raquez, P. Damman and P. Dubois, *Prog. Polym. Sci.*, 2012, **37**, 157.
33 Q. J. Yu, J. M. Xu and Y. Y. Han, *Appl. Surf. Sci.*, 2011, **258**, 1412.